



**HAL**  
open science

# Wideband Simulations of Periodic Structures by the Hybrid Spectral FDTD/TD-VFz Method

Samuel Gaucher, Christophe Guiffaut, Alain Reineix, Olivier Cessenat,  
Genevieve Maze-Merceur

► **To cite this version:**

Samuel Gaucher, Christophe Guiffaut, Alain Reineix, Olivier Cessenat, Genevieve Maze-Merceur. Wideband Simulations of Periodic Structures by the Hybrid Spectral FDTD/TD-VFz Method. IEEE Antennas and Wireless Propagation Letters, 2022, 21 (5), pp.933-937. 10.1109/LAWP.2022.3152410 . hal-03668219

**HAL Id: hal-03668219**

**<https://unilim.hal.science/hal-03668219>**

Submitted on 17 May 2022

**HAL** is a multi-disciplinary open access archive for the deposit and dissemination of scientific research documents, whether they are published or not. The documents may come from teaching and research institutions in France or abroad, or from public or private research centers.

L'archive ouverte pluridisciplinaire **HAL**, est destinée au dépôt et à la diffusion de documents scientifiques de niveau recherche, publiés ou non, émanant des établissements d'enseignement et de recherche français ou étrangers, des laboratoires publics ou privés.

# Wideband simulations of periodic structures by the Hybrid Spectral FDTD/TD-VFz Method

Samuel Gaucher, Christophe Guiffaut, *Member, IEEE*, Alain Reineix, *Member, IEEE*, Olivier Cessenat, and Geneviève Mazé-Merceur

**Abstract**—The Spectral FDTD (SFDTD) method is combined with the discrete-time time-domain vector fitting algorithm (TD-VFz) to analyze 3D periodic structures excited by oblique incident plane waves over a wide frequency band. The time signal reconstruction with TD-VFz produces an untruncated response over an infinite time window allowing an accurate spectral result, specially near the cut-off frequency separating the spectrum propagating wave region of evanescent wave region.

**Index Terms**—periodic boundary condition, finite-difference time-domain, oblique incidence, Spectral FDTD, time-domain vector fitting.

## I. INTRODUCTION

**M**ETAMATERIALS are used in many applications such as antennas, cloaking devices or radar cross section (RCS) reduction. Some of them are composed of periodic patterns. Thus, periodic Floquet boundary conditions (PBC) are applied in periodic directions such that only one unit cell needs to be analyzed instead of the entire structure. Particularly, the finite-difference time-domain (FDTD) is a good candidate to compute the unit cell because of its simplicity, efficiency and wideband capabilities. However when the incident angle is fixed, time-advanced solutions are required on boundaries. Various techniques exist to deal with this difficulty and [1] distinguishes them into two classes: ‘direct field methods’ and ‘field-transformation methods’.

Spectral FDTD (SFDTD) [2] [3] is a direct field method which keeps the usual electric field  $E$  and magnetic field  $H$  unknowns. Then, all existing FDTD models and processings can straightforwardly be adapted to the SFDTD. In this approach, the horizontal wavenumber is fixed rather than the incident angle. Then the implementation of PBC becomes simple because no time-advanced data are required. The best advantage of this technique is the ability to use the standard Yee scheme without restriction on the Courant-Friedrich-Levy (CFL) condition, which is not angle-dependent [2]. On the other hand, when the horizontal wavenumber is fixed, the SFDTD scheme simultaneously excites propagating wave and evanescent wave regions [2] which are separated by the cut-off frequency. As a result, a resonant behavior occurs and yields undamped oscillations in the time signal. Thus, its discrete

Fourier transform (DFT) provides an inaccurate frequency response. To remedy this, the SFDTD method with the ARMA post-processing has been developed in [4]. Starting from the same idea, we propose to combine the SFDTD scheme with the discrete-time time-domain vector fitting (TD-VFz) [5] extrapolation technique. This approach is very robust, guaranteed stable poles and is a much lower model order than ARMA [6].

The organization of this paper is as follows. The SFDTD method and the resonance problem are explained in Section II. In Section III, the resonance problem is solved and the eigen-frequency is identified when consider a homogeneous layer. A comparative study of the time signal extrapolation techniques TD-VFz, ARMA and matrix-pencil (MP) [7] was performed to deduce the good efficiency of the TD-VFz method. In Section IV, the hybrid SFDTD/TD-VFz scheme is presented. First, a simple methodology to construct the spectral response for an arbitrary incident angle is proposed: The mapping between the wavenumber to angle response is directly obtained by the TD-VFz rational transfer function. Secondly, a convolution perfectly matched layers (CPML) setting is given to avoid late-time divergence and to improve the accuracy near the cut-off frequency. In section V, two numerical examples are implemented to demonstrate the hybrid method performance. The hybrid method is compared to the Material Independent (MI) scheme [8] for verification. MI and SFDTD simulations are performed with the XLIM laboratory homemade Tensifd solver [9] and SFDTD temporal data are extrapolated with TD-VFz implemented in Matlab scripting.

## II. SPECTRAL FDTD REVIEW

Let us assume a  $(l_x, l_y)$  periodicity in the  $(x, y)$  directions with a  $z$ -propagation of an incident wave. Like [10], an arbitrary azimuth angle is chosen to  $\varphi = \varphi_0$ . Then, the horizontal wavenumber depends on the angular frequency  $\omega = 2\pi f$  and the elevation angle  $\theta$  as  $k_h = \omega \sin \theta / c_0$ .  $c_0$  is the speed of light in free space. As  $\varphi$ ,  $k_h$  is also fixed for one simulation of the SFDTD method. The constant components  $k_x$  and  $k_y$  of the plane wave vector  $k$  are deduced as a function of the azimuth angle and the horizontal wavenumber

$$k_x = k_h \cos \varphi_0, \quad k_y = k_h \sin \varphi_0. \quad (1)$$

By fixing them, simple time-domain PBC are found for  $\Psi = E$  or  $H$

$$\Psi(x, y, z, t) = \Psi(x + ml_x, y + nl_y, z, t) e^{j(k_x ml_x + k_y nl_y)}, \quad (2)$$

S. Gaucher and O. Cessenat are with Commissariat à l’Energie Atomique et aux Energies Alternatives (CEA-CESTA), Le Barp 33116, France, (e-mail: samuel.gaucher@cea.fr; olivier.cessenat@cea.fr).

S. Gaucher, C. Guiffaut and A. Reineix are with CNRS Limoges, XLIM, France, Limoges 87000, (email: samuel.gaucher@xlim.fr, christophe.guiffaut@xlim.fr, alain.reineix@xlim.fr).

This work is funded by the DGA AID and the CEA CESTA.

Manuscript received month day, year; revised month day, year.

where  $m$  and  $n$  are any integers. Then, SFDTD scheme is exactly the same as the FDTD one with complex E-H fields unknowns instead of real for the latter. We deduce from the expression  $\theta(\omega) = \arcsin \frac{k_h}{k_0}$  that different frequencies correspond to different incident angles, and for a positive real incidence, the condition  $k_0 \geq k_h$  must be verified. In other words, this is referred to the propagating wave region if  $f \geq f_c$  else to the evanescent wave region, where

$$f_c = \frac{c_0 k_h}{2\pi} \quad (3)$$

is the cut-off frequency. Because both the propagating wave region and the evanescent wave region are excited by the SFDTD method, surface waves are guided along horizontal directions at some frequencies called 'eigen-frequencies'. Thus, the energy of a horizontal wave continuously re-enters the computational domain through the PBC instead of being absorbed by the top and bottom CPML [2]. As a result, a resonance behavior occurs: temporal data do not converge and an accurate spectral response cannot be obtained by DFT.

To overcome this difficulty, [2] adopts a modulated Gaussian waveform to excite only the propagating wave region

$$\mathcal{F}_{inc}(t) = \exp \left[ -\frac{(t-t_0)^2}{T^2} \right] \exp(j2\pi f_0 t), \quad (4)$$

where  $t_0$  is the time delay,  $T$  the pulse width and the signal magnitude at  $f_c$  should be at least 40 dB lower than the signal level at the center frequency  $f_0$ . This simple approach improves the spectral response accuracy by attenuating the horizontal resonance. However, especially for very wideband excitation, there are still some artifacts near the cutoff frequency corresponding to high incident angles in the spectral domain. Moreover, only the propagating wave region is determined with this technique and not the surface wave region.

### III. EIGEN-FREQUENCIES IDENTIFICATION WITH TD-VFZ

Let us consider a homogeneous layer of thickness 9.375 mm and dielectric constant  $\epsilon_r = 4$ . FDTD simulation runs with  $k_h = 50$  rad/m,  $\varphi = 90^\circ$  and a Gaussian pulse excitation. The time domain reflected field of the fundamental mode on the interface between the air and the layer is shown in Fig. 1. Temporal data do not converge and oscillations are observed.

To obtain a correct spectral reflection coefficient  $\mathcal{R}$ , the ratio between the output (real part of the reflected field) and input (excitation) response is decomposed with TD-VFz [5], as a rational transfer function

$$\mathcal{R}(z = \exp[j\omega\Delta_t]) = d + \sum_{n=1}^M \frac{r_n}{1 - z^{-1}s_n}, \quad (5)$$

where  $d$  is a constant,  $r_n$  and  $s_n$  are the complex residues and poles respectively and  $\Delta_t$  is the time sample. Fig. 2 illustrates the reflection coefficient over a wideband from 0<sup>+</sup> GHz to 25 GHz obtained by the SFDTD scheme with the modulated Gaussian excitation (4) and a strong attenuation  $Att_{f_{max}} = 60$  dB at  $f_c$ , and by the SFDTD scheme combined with the extrapolation technique ARMA, MP or TD-VFz for the same  $M = 18$  poles number ( $p = q = 18$  for

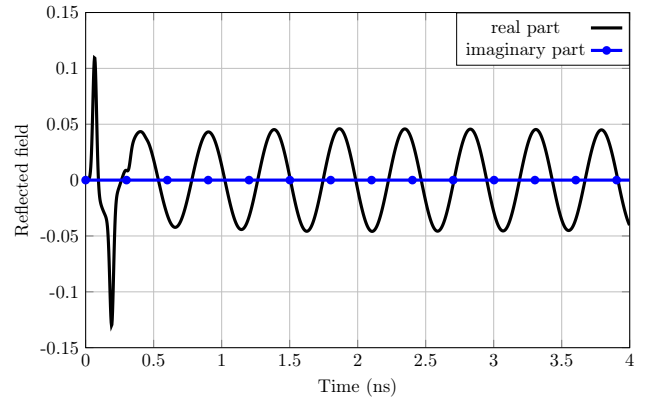


Fig. 1: Reflected wave in the time domain. Resonance behavior is observed.

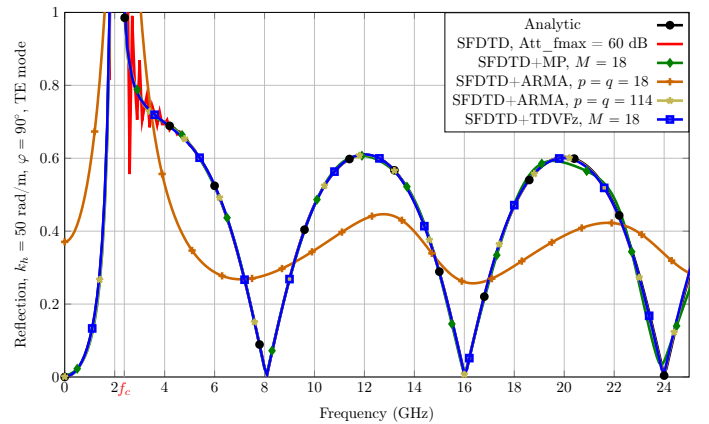


Fig. 2: Reflection coefficient for the homogeneous layer.

ARMA [4]) and 5 iterations for TD-VFz poles convergence. The FDTD spatial steps are all equal to  $\Delta = 0.1875$  mm and CFL = 0.99. Excellent agreement is observed between the hybrid SFDTD/TD-VFz method and analytical reference, especially near the cut-off frequency, on the contrary to the alone Spectral FDTD scheme where the response is noisy. The MP technique gives a good result but with an accuracy loss for high frequencies. In addition, the number of poles is insufficient for the ARMA method which does not give the expected result. An interesting point consists in the eigen-frequencies identification. When (5) gives poles on the unit circle boundary, resonances occur and eigen-frequencies are identified. For the sample  $k_h = 50$ , there is only one reported in the Table I for several extrapolation techniques and poles number choices. For the order  $M = 18$ , the best matching with theory is obtained with the SFDTD/TD-VFz scheme. We note that  $p = q = 114$  for ARMA are required to obtain the same result as TD-VFz with  $M = 18$ . Furthermore,  $M = 24$  gives the same excellent result for MP and TD-VFz but  $M < 24$  for MP gives an inaccurate response at high frequencies. Regarding the CPU time, ARMA ( $p = q = 114$ ) has a slightly faster calculation time than TD-VFz ( $M = 18$ ) and MP is a slower method. Also the memory usage is 30 MB for ARMA and TD-VFz, and 100 MB for MP ( $M = 18$ ).

TABLE I: Eigen-frequency prediction. The theory gives  $f_r = 2.0751$  GHz.

	Prediction (GHz)	Error (%)	CPU time (s)
ARMA (p=q=18)	2.2614	8.978	0.06
MP (M=18)	2.0758	0.034	3.3
TD-VFz (M=18)	2.0746	0.024	1.38
MP (M=24)	2.0752	0.005	3.11
TD-VFz (M=24)	2.0752	0.005	1.64
ARMA (p=q=114)	2.0746	0.024	1.2

#### IV. HYBRID SPECTRAL-FDTD/TD-VFz

##### A. Mapping $\mathcal{R}(0 < k_h, f)$ to $\mathcal{R}(0 < \theta, f)$

The normal incidence case  $\theta = 0^\circ$  is trivial and corresponds to  $k_h = 0$ . To deal with the oblique incident angles for the frequency band  $[0 < f_{min}, f_{max}]$  and incident angle range  $[0 < \theta_{min}, \theta_{max}]$  of interest, we first calculate the extremum horizontal wavenumber as

$$k_{h_{max}} = \frac{2\pi f_{max}}{c_0} \sin \theta_{max}, \quad k_{h_{min}} = \frac{2\pi f_{min}}{c_0} \sin \theta_{min}. \quad (6)$$

To compute the reflection coefficient as a function of the incident angle, we run the FDTD simulation for the  $N$  samples of  $k_h^i$  with the fixed azimuth angle  $\varphi = \varphi_0$

$$k_h^i = k_{h_{min}} + i \frac{k_{h_{max}} - k_{h_{min}}}{N-1}, \quad i = 0, \dots, N-1, \quad (7)$$

by using (1) to determine the phase values in the PBC formulation (2). Then, each response with sample  $k_h^i$  is extrapolated by the M-order TD-VFz algorithm to obtain the M residues  $r_n^i$  and poles  $s_n^i$ , and the constant  $d^i$ . After that, an incident angle-reconstruction is applied. For a given angle  $\theta_{min} \leq \theta_j \leq \theta_{max}$ , we compute the  $N$  frequencies

$$f^i = \frac{ck_h^i}{2\pi \sin \theta_j}, \quad i = 0, \dots, N-1. \quad (8)$$

The reflection coefficient  $\mathcal{R}$  evaluated at angle  $\theta_j$  is calculated with the transfer function (5) for all frequencies  $f^i$

$$\mathcal{R}(f^i, \theta_j) = d^i + \sum_{n=1}^M \frac{r_n^i}{1 - \exp[-j2\pi f^i \Delta_t] s_n^i}. \quad (9)$$

As frequencies are imposed by the formula (8), the Lagrange interpolation is used to obtain the reflection coefficient at the desired frequencies. Assuming a desired frequency  $f^i \leq \tilde{f} \leq f^{i+1}$ , the reflection coefficient for the angle  $\theta_j$  and frequency  $\tilde{f}$  is given by

$$\mathcal{R}(\tilde{f}, \theta_j) = \frac{f^{i+1} - \tilde{f}}{f^{i+1} - f^i} \mathcal{R}(f^i, \theta_j) + \frac{\tilde{f} - f^i}{f^{i+1} - f^i} \mathcal{R}(f^{i+1}, \theta_j). \quad (10)$$

##### B. CPML setting

The stretched-coordinate metrics  $s_z$  of the complex frequency shifted CPML (CFS-CPML) approach [11] is defined in the z-direction as

$$s_z = \kappa_z + \frac{\sigma_z}{\alpha_z + j\omega\epsilon_0}, \quad (11)$$

where  $\sigma_z$  is the conductivity depending of the z-depth layer of the CPML to provide absorption for propagating waves. Parameters  $\kappa_z$  and  $\alpha_z$  better attenuate the evanescent waves at low frequencies, by stretching the FDTD spatial step with  $s_z$  as can be seen by taking the limit  $\omega \rightarrow 0$ . In this paper, the parameter  $\alpha_z$  is constant with the PML cut-off frequency defined by

$$f_c^{PML} = \frac{\alpha_z}{2\pi\epsilon_0}. \quad (12)$$

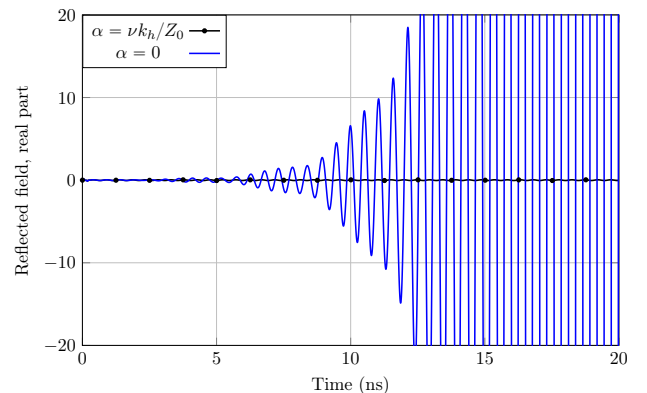
The condition  $f_c^{PML} < f_c$  is a good compromise for absorbing propagative waves without neglecting the absorption of evanescent waves. Then, we propose

$$f_c^{PML} = \nu f_c, \quad (13)$$

where  $\nu$  should be a real between 0.15 and 0.75 according to our numerical experiences. The constant  $\alpha_z$  profile in CPML is found by using (3)

$$\alpha_z = \nu \frac{k_h}{Z_0}, \quad (14)$$

where  $Z_0 \approx 376.730 \Omega$  is the impedance in free space. It is important to have  $\alpha_z > 0$  to avoid late-time divergence. The real part of the time domain reflected field for the same case as section III and during a long time simulation of 20 ns is shown in Fig. 3 for two  $\alpha_z$  values. Time domain signal diverges when  $\alpha_z = 0$  but the setting (14) with  $\nu = 0.75$  efficiently corrects the problem. On the other hand, the conductivity grows geometrically in CPML because it is the best profile for lowering the reflection of the evanescent waves [12]. Moreover, it is very interesting to enhance the absorption of the waves at grazing incidence since they are close to the cut-off frequency and therefore disturbed by the resonance frequencies. Consequently for a CPML of 12 cells in thickness, we adopt the optimum geometrical expansion  $g = 1.9$  with the theoretical normal incidence reflection coefficient expected at the interface between air and CPML equals to  $R(0) = 10^{-14}$ . Theses setting are obtained from the PML theoretical reflection of [13]. Therefore PML outperforms for grazing incidence wave absorption. The counterpart can be a lesser absorption for normal incidence or weak incidence angle waves but the reflection coefficient remains below -50 dB. Besides this behaviour is stable with the frequency.


 Fig. 3: Time domain signal for two values of  $\alpha$  ( $k_h = 50$ ).

## V. NUMERICAL RESULTS

For the two numerical examples of this section, periodic solvers run with a 2 ns simulation time and TD-VFz with  $M = 40$  poles and 15 iterations for the poles convergence. The setting (14) with  $\nu = 0.35$  is chosen for all simulations.

### A. Pattern composed of two homogeneous lossy layers

Let us consider a stratified media composed of two arbitrary homogeneous layers. The geometry, dimensions and parameters of the layers are plotted in Fig. 4 (a). The model is simulated by using the proposed method for  $N = 100$  horizontal wavenumber samples with  $f_{max} = 10$  GHz,  $\theta_{max} = 80^\circ$ ,  $\Delta = 0.2$  mm and CFL = 0.99. The numerical reflection coefficient and phase magnitude for the TE mode with a constant azimuth angle  $\varphi = 90^\circ$  is compared to the theory [14] as shown in Fig. 5 and Fig. 6 respectively. A very good agreement with theoretical data is observed for many incident angles. Note that the accuracy is less good at high incidence angles  $60^\circ$  and  $80^\circ$  for low frequencies (8) below 0.5 GHz approximately due to the strong proximity of them with the cut-off frequency.

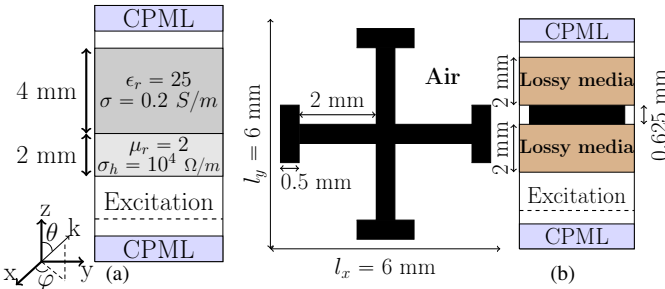


Fig. 4: Unit cell geometry. (a) two homogeneous layers, ( $yOz$ ) plane. (b) JCFSS, left: ( $xOy$ ) plane, right: ( $yOz$ ) plane.

### B. Jerusalem Cross FSS with anisotropic and lossy media

The Jerusalem cross [8] is a perfect electromagnetic conductor (PEC) between two anisotropic and lossy FSS media with relative permittivity and conductivity diagonal tensors given by  $\epsilon_r = \text{diag}(2.2, 1.1, 1.5)$  and  $\sigma = \text{diag}(0.05, 0.03, 0.01)$ . Pattern geometry is plotted in Fig. 4 (b). The model is

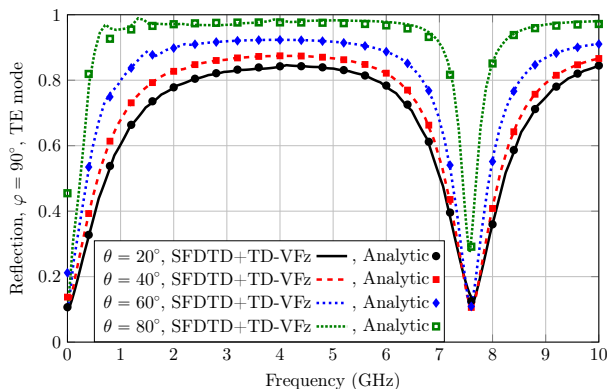


Fig. 5: Reflection coefficient magnitude for the two layers.

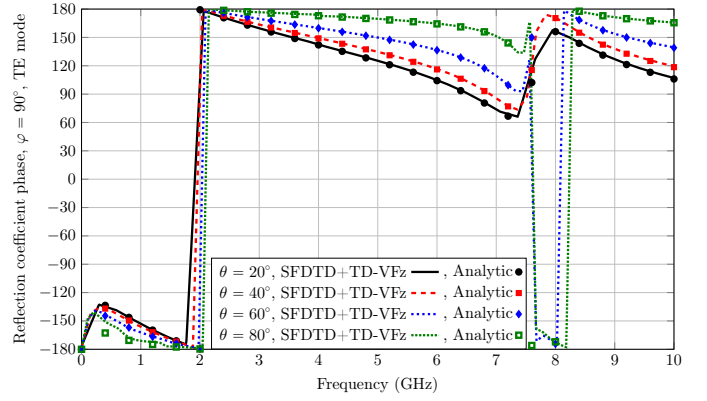


Fig. 6: Reflection coefficient phase for the two layers.

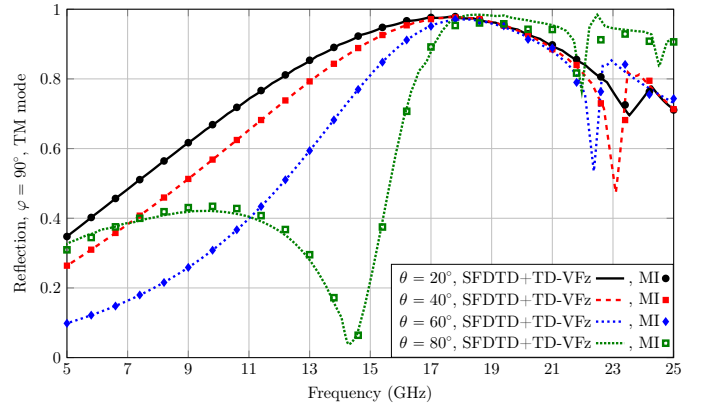


Fig. 7: Reflection coefficient magnitude for the JCFSS.

simulated by using the proposed method for  $N = 100$  horizontal wavenumber samples over a wideband from 5 GHz to 25 GHz with  $\theta_{max} = 80^\circ$ ,  $\Delta = 0.125$  mm and CFL = 0.99. Considering the TM mode and a constant azimuth angle  $\varphi = 90^\circ$ , very good agreement between the hybrid and MI scheme is observed in Fig. 7 for various incident angles. Note that the CFL condition of the MI field transformation method is  $c_0\sqrt{3}\Delta_t \leq \Delta(1 - \sin\theta)$ . Thus, the simulation time becomes prohibitively long at high incidence. The best advantage of the hybrid method is that the CFL condition is the same for each horizontal wavenumber sample  $k_h$  as  $c_0\sqrt{3}\Delta_t \leq \Delta$  [2].

## VI. CONCLUSION

The Spectral FDTD scheme combined with the TD-VFz decomposition is an efficient hybrid approach to analyze periodic structures excited by oblique incident plane waves without reducing the CFL stability criterion of the FDTD method. The VF-poles perfectly fit the response resonant modes allowing the hybrid method to deal with high incident angles. CFS-PML is successfully used to avoid late time instabilities with a simple setting of the low-frequency stretching coefficient  $\alpha$  from the cut-off frequency of the PBC. In addition, the PML conductivity profile is optimized for grazing incident angle increasing the accuracy computation of the reflection coefficient.

## REFERENCES

- [1] A. Taflove and S. C. Hagness, *Computational electrodynamics: the finite-difference time-domain method*, 3rd ed. Artech house, 2005.
- [2] F. Yang, J. Chen, R. Qiang, and A. Elsherbeni, "A simple and efficient FDTD/PBC algorithm for scattering analysis of periodic structures," *Radio Science*, vol. 42, no. 04, pp. 1–9, 2007.
- [3] A. Aminian and Y. Rahmat-Samii, "Spectral FDTD: a novel technique for the analysis of oblique incident plane wave on periodic structures," *IEEE Trans. Antennas Propag.*, vol. 54, no. 6, pp. 1818–1825, 2006.
- [4] F. Yang, A. Elsherbeni, and J. Chen, "A hybrid spectral-FDTD/ARMA method for periodic structure analysis," in *2007 IEEE Antennas and Propag. Society International Symposium*, 2007, pp. 3720–3723.
- [5] C.-U. Lei and N. Wong, "Efficient linear macromodeling via discrete-time time-domain vector fitting," in *21st International Conference on VLSI Design (VLSID 2008)*. IEEE, 2008, pp. 469–474.
- [6] A. Ubolli and B. Gustavsen, "Comparison of methods for rational approximation of simulated time-domain responses: ARMA, ZD-VF, and TD-VF," *IEEE Trans. Power Del.*, vol. 26, no. 1, pp. 279–288, 2010.
- [7] T. Sarkar and O. Pereira, "Using the matrix pencil method to estimate the parameters of a sum of complex exponentials," *IEEE Antennas Propag. Mag.*, vol. 37, no. 1, pp. 48–55, 1995.
- [8] B. Liang, M. Bai, H. Ma, N. Ou, and J. Miao, "Wideband analysis of periodic structures at oblique incidence by material independent FDTD algorithm," *IEEE Trans. Antennas Propag.*, vol. 62, no. 1, pp. 354–360, 2014.
- [9] *Time ElectroMagnetic Simulator-Finite Difference Software, TEMSI-FD*, CNRS, Univ. Limoges, Limoges, France, 2006.
- [10] Y.-J. Zhou, X. Zhou, T.-J. Cui, R. Qiang, and J. Chen, "Efficient simulations of periodic structures with oblique incidence using direct spectral FDTD method," *Progress In Electromagnetics Research*, vol. 17, pp. 101–111, 2011.
- [11] J. A. Roden and S. D. Gedney, "Convolution PML (CPML): An efficient FDTD implementation of the CFS–PML for arbitrary media," *Microwave and optical technology letters*, vol. 27, no. 5, pp. 334–339, 2000.
- [12] J.-P. Bérenger, "An optimized CFS-PML for wave–structure interaction problems," *IEEE Trans. Electromagn. Compat.*, vol. 54, no. 2, pp. 351–358, 2011.
- [13] J.-P. Bérenger, "Evanescent waves in PML's: Origin of the numerical reflection in wave-structure interaction problems," *IEEE Trans. Antennas Propag.*, vol. 47, no. 10, pp. 1497–1503, 1999.
- [14] K. Demarest, R. Plumb, and Z. Huang, "FDTD modeling of scatterers in stratified media," *IEEE Trans. Antennas Propag.*, vol. 43, no. 10, pp. 1164–1168, 1995.